MAGLEV 2022
25th International Conference on Magnetically Levitated Systems and Linear Drives

Simulation of a High-Speed Maglev Train on an Elastic Guideway of Infinite Length

Georg Schneider[1], Patrick Schmid[1], Arnim Kargl[1],
Xin Liang[2], Florian Dignath[3], and Peter Eberhard[1]

[1] Institute of Engineering and Computational Mechanics, University of Stuttgart, Stuttgart, Germany
[2] CRRC Qingdao Sifang Co., Ltd., Qingdao, People's Republic of China
[3] thyssenkrupp Transrapid GmbH, Munich, Germany
Corresponding author: Georg Schneider (e-mail: georg.schneider@itm.uni-stuttgart.de)

***Abstract*—Simulations of the coupled vehicle/guideway dynamics are an essential part in the development of high-speed magnetic levitation (maglev) systems with higher speed than traveled so far. In this contribution, a two-dimensional rigid multibody model mapping the heave-pitch motion of the vehicle is presented and used for dynamics simulations of the vehicle traveling along an infinite elastic guideway. The concept of moving system boundaries is applied for the guideway model to efficiently implement an infinite series of elastic Euler-Bernoulli beams while keeping the number of system states small. Guideway deflection interpolation and computation of equivalent nodal forces and torques are realized using Hermite polynomials. Together with a physically advanced magnet model and a model predictive control scheme, the coupled system is applied for vehicle and guideway dynamics analysis for different vehicle speeds and guideway elasticities.**

***Index Terms*—Flexible Multibody System, High-Speed Maglev, Infinite Elastic Guideway, Transrapid.**

I. Introduction

The worldwide only commercial high-speed maglev train based on electromagnetic suspension technology is implemented at the Shanghai Maglev Transportation line between Pudong International Airport and Longyang Road Station with a maximum speed of 430 km/h. Currently, a new high-speed maglev train with a maximum speed of 600 km/h is under development at the Chinese rolling stock manufacturer CRRC Qingdao Sifang Co., Ltd. A prototype of the future vehicle has been presented to the public in May 2019 and it traveled along a short test track with low speed in July 2021. The new high-speed maglev train will close the gap between current high-speed railway technology with top speeds of 300 to 350 km/h and aircraft traveling with speeds around 900 km/h, and, therefore, offers a notable alternative for short to medium-haul flights with respect to economic and ecologic aspects.

One main cost factor of a high-speed maglev system is the track consisting of hundreds of kilometers of guideway. The dynamic behavior of this guideway has a significant impact on the requirements of the vehicle control system. The deflection of the guideway girders in relation to their length and the vehicle speed needs to be small in order to prevent strong coupling with the vehicle dynamics. To verify this requirement, the system analysis has to consider the dynamical behavior of the coupled system consisting of the guideway and vehicle mechanics as well as the magnet and controller dynamics.

The coupled dynamics of vehicle and guideway is modeled and investigated in several previous publications with various approaches. In early approaches, when guideway elasticity is considered, the vehicle models cover a range from a single concentrated mass to a few distributed constant forces [1,2,3]. For more detailed rigid multibody vehicle models, the guideway is considered either stiff [4,5] or as one single elastic guideway element [6].

Simulations of a multibody maglev vehicle crossing a single flexible beam with high velocity show that the elastic deformation of the beam causes a disturbance that influences the vehicle dynamics for several seconds after the vehicle has left the elastic guideway element [6]. Thus, to investigate the interaction of disturbances for a traveling vehicle caused by multiple elastic guideway elements in a row, as it is the case for elevated guideways supported on rigid pillars, several flexible beam elements are required in the simulation model as well. In the past, for such detailed guideway models with several girders, quite simple vehicle models were used. In the contribution at hand, a more detailed two-dimensional multibody vehicle traveling on a pillared flexible guideway of infinite length is modeled, simulated, and analyzed. Thereby, different aspects of guideway modeling are examined. First, a model for a single elastic guideway element is set up and coupled with a passing vehicle as published in [6]. Each elastic guideway element is modeled as single-span Euler-Bernoulli beam. Forces applied at arbitrary positions on the discretized beam are replaced by equivalent nodal forces and torques acting at its nodes. Second, some of these guideway elements are combined systematically to obtain an infinite series of elastic guideway elements as published in [7]. For computational efficiency, only the guideway elements occupied by the vehicle are considered to keep the dimension of the equations of motion as small as possible. Thus, the boundaries of the simulated system are shifted along the guideway with the moving vehicle.

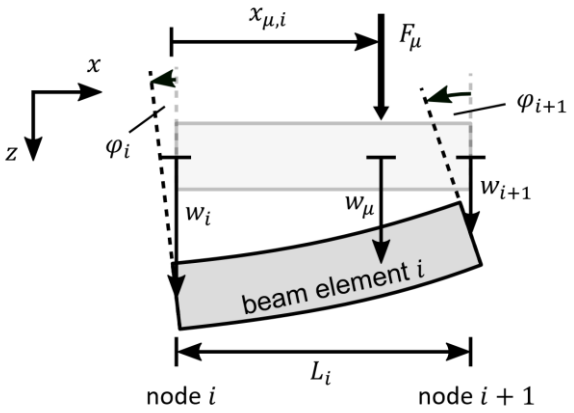

Fig. 1. Beam deflection w_μ is obtained by interpolating the deflections and rotations at the adjacent nodes.

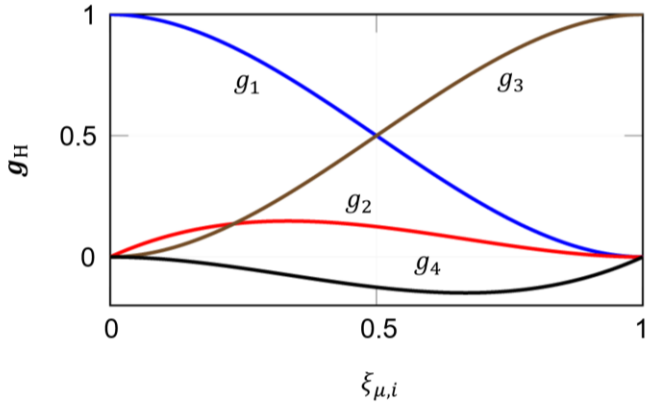

Fig. 2. Third-order Hermite polynomials $\boldsymbol{g}_\mathrm{H} = [g_1, g_2, g_3, g_4]^\mathrm{T}$ plotted for $0 \le \xi_{\mu,i} \le 1$.

The equations of motion for the mechanical parts are obtained in symbolic form from the Matlab-based multibody simulation toolbox Neweul-M^2 [8] and are coupled in Simulink with the dynamic equations of the electromagnets and the magnet controllers. The resulting vehicle and guideway dynamics are analyzed with respect to control behavior and ride comfort aspects.

II. Guideway Model

The guideway is modeled as an infinite series of identical elastic Euler-Bernoulli beams supported on rigid pillars at their ends. In the following subsections, first the model of a single guideway element is described, before a small number of identical guideway elements is combined systematically to obtain an infinite series of elastic guideway elements.

Each beam representing a guideway element is parameterized according to the first generation of concrete guideway at the former Transrapid test facility in Northern Germany (TVE) as provided by [9]. The beams are 24.768 m long and discretized by 24 finite beam elements. To allow asymmetric shapes of the beams, they are reduced to their first three eigenmodes, which is a sufficiently accurate approximation as stated in [3]. Rotational inertia and shear deformations of the beam can be neglected in this case according to [10], which justifies applying the Euler-Bernoulli beam theory. The deflection at mid span caused by the beams own weight is 8.6 mm which matches the analytical solution. Its first natural frequency is 6 Hz. The Euler-Bernoulli beams are created and reduced using the Matlab-based model order reduction toolbox MatMorembs, developed at the Institute of Engineering and Computational Mechanics, and then included as flexible body in Neweul-M^2.

A. Single Elastic Guideway Element

The partial differential equation describing an Euler-Bernoulli beam as given in [10], for example, reads as

$$EI\, w''''(x,t) + \rho A\, \ddot{w}(x,t) = \textstyle\sum_\mu F_\mu(t)\, \delta\big(x - x_\mu\big)\,. \qquad (1)$$

The vertical deflection w depends on time t and position x with $0 \le x \le L$, where L denotes the beam length. The beam deflection's fourth derivative in space is denoted as $w''''(x,t) \equiv \partial^4 w/\partial x^4$ and the second derivative in time as $\ddot{w}(x,t) \equiv \partial^2 w/\partial t^2$, respectively. The homogeneous beam has a constant bending stiffness EI, density ρ, and cross-sectional area A. The moving forces $F_\mu(t), \mu = 1(1)m$, where m is the number of magnet forces acting on the beam, act in vertical direction at positions x_μ, which is considered by means of the Dirac function $\delta(\,)$.

1) *Deflection Interpolation*

Since the magnetic force F_μ depends on the air gap between the magnet and the guideway, the deflection w_μ of the guideway is required right at the position where the magnet force applies. However, the continuous beam is implemented as a discretized finite element Euler-Bernoulli beam model with 24 beam elements, 25 nodes, and cubic shape functions for the beam deflection. Therefore, beam deflections are only computed at the nodes of the finite elements. To obtain the deflection w_μ at an arbitrary position of a beam element i, which is in general between two nodes, the deflections $w_{\{i,i+1\}}$ and rotations $\varphi_{\{i,i+1\}}$ of the adjacent nodes i and $i+1$ are interpolated, see Fig. 1. The interpolation is implemented by means of the third-order Hermite polynomials

$$\boldsymbol{g}_\mathrm{H} = \begin{bmatrix} g_1 \\ g_2 \\ g_3 \\ g_4 \end{bmatrix} = \begin{bmatrix} 1 - 3\xi_{\mu,i}^2 + 2\xi_{\mu,i}^3 \\ \xi_{\mu,i} - 2\xi_{\mu,i}^2 + \xi_{\mu,i}^3 \\ 3\xi_{\mu,i}^2 - 2\xi_{\mu,i}^3 \\ -\xi_{\mu,i}^2 + \xi_{\mu,i}^3 \end{bmatrix}, \qquad (2)$$

$$\xi_{\mu,i} = \frac{x_{\mu,i}}{L_i}\,, \qquad 0 \le x_{\mu,i} \le L_i\,,$$

plotted in Fig. 2, resulting from a third-order polynomial ansatz function and the boundary conditions at the nodes [11]. Therefore, the beam deflection at an arbitrary position reads

$$w_\mu = [w_i, -L_i\varphi_i, w_{i+1}, -L_i\varphi_{i+1}]\, \boldsymbol{g}_\mathrm{H}\,. \qquad (3)$$

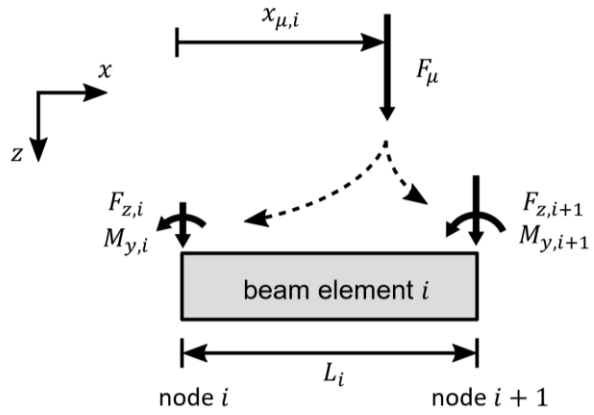

Fig. 3. Force F_μ acting on a beam element is replaced by equivalent nodal forces and torques acting on the neighboring nodes.

2) *Equivalent Nodal Forces and Torques*

On the other hand, forces can be transmitted to the discretized beam only at its nodes. Therefore, a vertical force F_μ, acting on beam element i with length L_i between nodes i and $i+1$, needs to be replaced by equivalent forces and torques acting at the neighboring nodes, see Fig. 3. According to [11], the principle of conservation of virtual work must be observed for the derivation of the vector of equivalent nodal forces and torques $\boldsymbol{p}_{\mathrm{equ},i} = \left[F_{z,i}, M_{y,i}, F_{z,i+1}, M_{y,i+1}\right]^{\mathrm{T}}$. That means, F_μ with its virtual deflection δw_μ has to do the same virtual work δW as the equivalent nodal forces and torques $\boldsymbol{p}_{\mathrm{equ},i}$ with their respective virtual deflections and rotations $\delta \boldsymbol{w}_{\mathrm{nod},i}$, leading to the equation

$$\delta W = \delta w_\mu \, F_\mu \stackrel{!}{=} \delta \boldsymbol{w}_{\mathrm{nod},i}^{\mathrm{T}} \, \boldsymbol{p}_{\mathrm{equ},i} \,, \tag{4}$$

resulting in the vector of equivalent nodal forces and torques

$$\boldsymbol{p}_{\mathrm{equ},i} = \begin{bmatrix} F_{z,i} \\ M_{y,i} \\ F_{z,i+1} \\ M_{y,i+1} \end{bmatrix} = \begin{bmatrix} F_\mu & 0 & 0 & 0 \\ 0 & -F_\mu L_i & 0 & 0 \\ 0 & 0 & F_\mu & 0 \\ 0 & 0 & 0 & -F_\mu L_i \end{bmatrix} \boldsymbol{g}_{\mathrm{H}} \,. \tag{5}$$

B. Infinite Series of Elastic Guideway Elements

In order to run simulations of a maglev vehicle on a regularly pillared elastic track, a small number of identical beams as described above are used repeatedly by applying the concept of moving system boundaries as described in [10] and illustrated in Fig. 4. The basic idea is to take a beam from behind the vehicle after the vehicle left it and it is no longer needed there, reset its states so that it is plane and in rest, and put it in front of the vehicle to be entered by the vehicle again. Thereby, the number of system states is kept small and an infinite series of elastic guideway elements can be implemented efficiently.

The number of beams required for the model is at least the number of guideway elements covered by the vehicle

$$n_{\mathrm{covered}} = \lceil l_{\mathrm{vehicle}} / l_{\mathrm{beam}} \rceil + 1 \tag{6}$$

with the overall vehicle length l_{vehicle}, single beam length l_{beam}, and the ceiling function $\lceil x \rceil$, mapping x to the least integer greater than or equal to x. Guideway elements ahead of or behind the vehicle do not have to be considered since the guideway elements are supported by the rigid pillars in such a way that they are decoupled from each other. Therefore, no guideway dynamics occurs for the beams ahead of the vehicle, like traveling waves, for example, and the decaying oscillations of the beams behind the vehicle do not have any influence on the vehicle dynamics. Nevertheless, two additional beams are required for the implementation due to technical reasons. For further explanations see [7]. Thus, the minimum number of beams required for the guideway model is

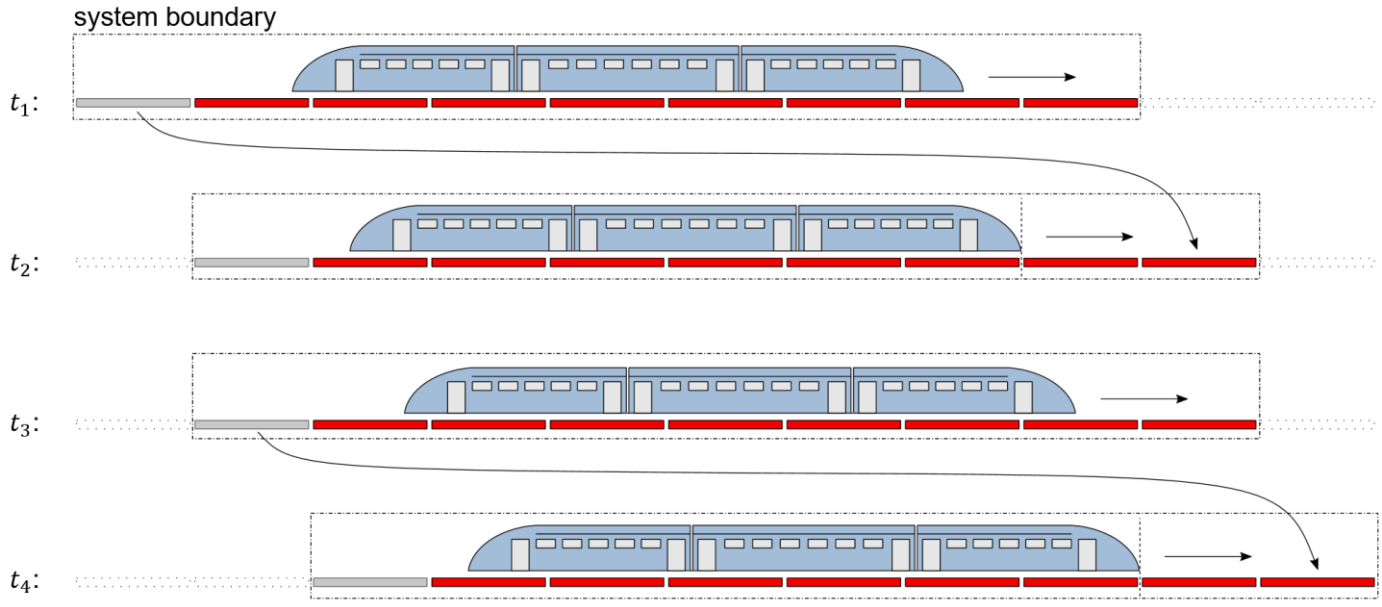

Fig. 4. Concept of moving system boundaries: A small number of guideway elements is used repeatedly to realize an infinitely long elastic guideway and keep the number of system states small at the same time.

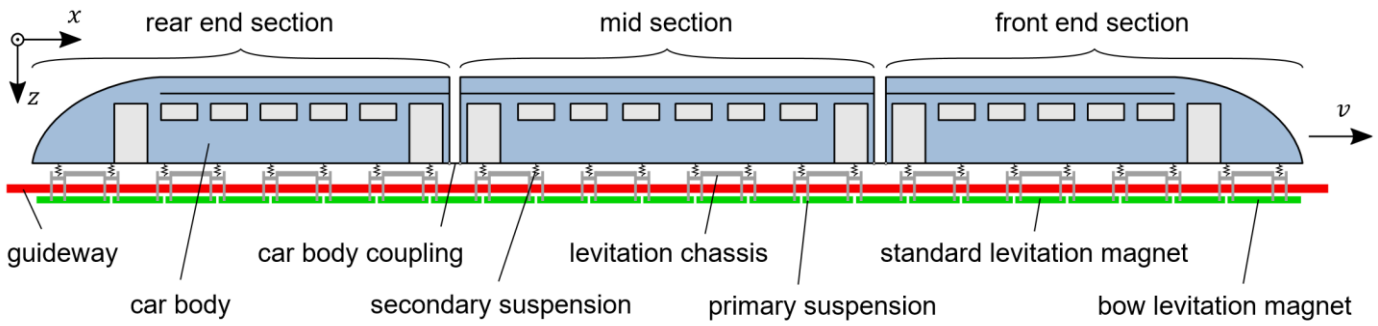

Fig. 5. Components of the complete vehicle model consisting of three sections on the guideway.

$$n_{\text{required}} = n_{\text{covered}} + 2\,. \tag{7}$$

However, an arbitrary number of additional beams may be added to the model, for example to observe and analyze the decaying guideway vibrations for some time after the vehicle left a beam. For a vehicle dynamics analysis, no additional guideway elements behind the vehicle are necessary.

III. Vehicle Model

The vehicle is modeled as a two-dimensional rigid multibody system representing a longitudinal cut through the system in the x-z-plane mapping the heave-pitch motion, see Fig. 5. The modeled vehicle comprises three sections, that is, two end sections and one mid section. Each section consists of rigid bodies, namely a car body, four levitation chassis and several levitation magnets. Each of these bodies has two degrees of freedom, a translational one in vertical direction, allowing heave motion, and a rotational one about the y-axis, allowing pitching. Thus, the vehicle model has 76 mechanical degrees of freedom in total.

The levitation magnets and the levitation chassis are connected by quite stiff elastomer elements, also called primary suspension. The levitation chassis are coupled to their respective car body by relatively soft air springs, the so-called secondary suspension, which to a great extent decouples the passenger cabin in the car body from the higher frequency vibrations of the magnets and levitation chassis. Both connections are modeled as linear spring-damper force elements.

The vehicle and guideway are coupled by attractive electromagnetic forces acting between the levitation magnets on vehicle side and stator packs installed on the bottom side of the guideway pulling the vehicle towards the guideway from below. As described in the subsequent section, the magnet model provides one concentrated magnetic force per half magnet, which is used as input to the mechanical model. Therefore, two force elements are implemented for each standard levitation magnet in the mechanical vehicle model. For the bow levitation magnets, which are longer and simplified by three half magnets, thus three magnetic forces are applied.

IV. Magnet Model and Controller

The magnet model used here is described in detail in [12]. It is an advanced model including the physical effects of magnetic reluctances, fringing and leakage flux, magnetic saturation, and eddy currents. Two different magnet model variants are available regarding the magnet force discretization. The first variant provides a fine discretization with one magnetic force at each of the twelve poles of a standard levitation magnet. For this variant, the electromagnet dynamics is described by a set of differential-algebraic equations (DAEs), which is time-consuming to solve and thus unsuitable for application in vehicle dynamics simulations with multiple magnets involved. The second variant provides a coarse discretization with one concentrated substitute magnetic force per half magnet. Here, the electromagnet dynamics is described by an ordinary differential equation (ODE), or two ODEs for a complete standard levitation magnet, respectively. Solving them takes significantly less time and, therefore, makes this magnet model variant suitable to be used for vehicle dynamics simulations with large vehicle models. The simplified model variant with the coarse discretization and the detailed one with the fine discretization have nearly the same input-output structure and an almost identical static and dynamic behavior. They are validated for the operational range of a Transrapid's levitation magnet in [12]. Furthermore, in [13] both magnet model variants are applied to the same mechanical models and with the same MPC scheme as in the contribution at hand. It is shown that the simulation results with the simplified magnet model with the coarse discretization are in excellent accordance with the results obtained with the detailed magnet model with the fine discretization. At the same time, the simulation time for the complete vehicle model is about 100 times faster with the coarse model.

The system based on electromagnetic suspension technology, that means, attractive magnetic forces, is inherently unstable. The levitating vehicle needs to be stabilized by actively controlling the electromagnetic forces to keep the air gap in a safe range and avoid contact of vehicle and guideway. For this purpose, each half magnet is controlled by its own magnet control unit. For the contribution at hand, an offset-free model predictive control (MPC) scheme from [14] is used, which is found suitable for controlling a Transrapid vehicle.

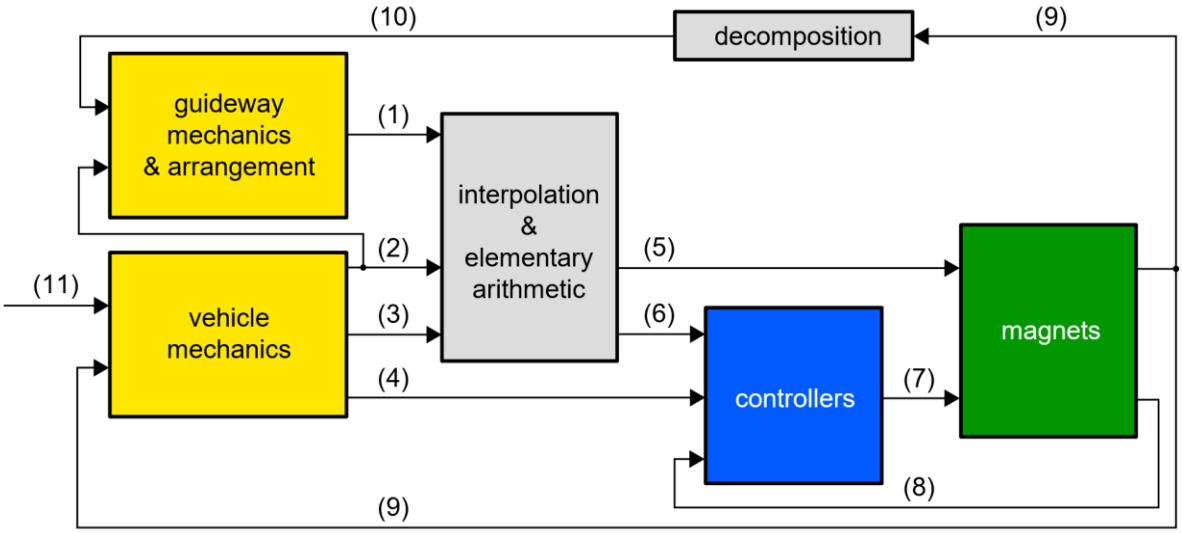

Fig. 6. Schematic setup of the coupled model in Simulink. (1) Nodal coordinates and velocities of beams, (2) x-positions of magnet forces, (3) magnet z-positions and velocities at magnet force application points (FAPs), x-positions of gap measurement units (GMUs), magnet z-positions at GMUs, (4) magnet z-accelerations at GMUs, (5) air gaps and air gap velocities at magnet FAPs, (6) air gaps at GMUs, (7) magnet voltages, (8) magnet currents, (9) magnet forces, (10) nodal forces and torques, (11) x-position of front end car body. For more details see [7].

V. Coupled System

All subsystems making up the model are coupled in Simulink. Figure 6 shows the schematic block diagram. The equations of motion for the mechanical vehicle and guideway models are derived in an automated manner by the in-house multibody modeling and simulation toolbox Neweul-M^2 using the Newton-Euler formalism. They are exported as C code and compiled as mex files that are included as S-functions in Simulink in the yellow blocks. The blue and green blocks contain the controller and magnet dynamics, respectively. Numerous input and output signals described in Fig. 6 connect the subsystems forming the complete coupled system. For further explanations regarding the coupled system see [7].

VI. Simulation Results

This section summarizes the simulation results obtained with the model described above that are published in [7]. The vehicle model is parameterized to represent the Transrapid TR08, while the guideway parameters are taken from the first generation of concrete guideway at the TVE. The beams are plane when they are unloaded and in rest, that is, when the only force acting on them is their own weight. In the investigated scenario, the vehicle travels with different constant velocities along the regularly pillared infinite elastic guideway.

Three aspects are examined, namely 1) the guideway dynamics below a passing vehicle, 2) the air gap control accuracy and the magnet motion at different positions along the vehicle, and 3) the influence of guideway stiffness on the mechanical magnet dynamics.

A. Guideway Dynamics

The deflection w_{mid} of a single guideway element at mid span is plotted in Fig. 7 over the position $x_{\mathrm{MF,front}}$ of the foremost magnet force for the vehicle traveling along the guideway with different velocities from 18 km/h (considered as quasi-static) to 600 km/h. The foremost magnetic force enters the beam at $x_{\mathrm{MF,front}} = 0$ and leaves it again at the first dashed vertical line. Then the beam is completely covered by the vehicle until the second dashed line, where the rearmost magnetic force enters the beam. At the last dashed line, the rearmost magnetic force leaves the beam so that the beam then is uncovered and can oscillate freely.

In the quasi-static case, the deflection increases while the vehicle enters the beam up to a value of approximately 6 mm when the beam is covered completely, and decreases again to zero when the vehicle leaves. The higher the velocity of the passing vehicle, the more severe overshoots and oscillations are visible, meaning more challenging disturbances for the controllers at the mid and rear vehicle sections to deal with. The reason for the overshoots due to loading and unloading of the beam is a more and more step-like shape of the load acting on the beam over time with increasing vehicle speed. Since the bending of an Euler-Bernoulli is described by a partial differential equation of second order in time, see (1), the

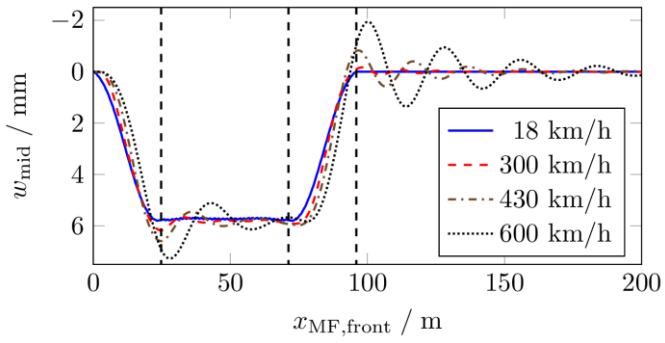

Fig. 7. Deflection of a single guideway element at mid span versus position of the foremost magnetic force for various velocities.

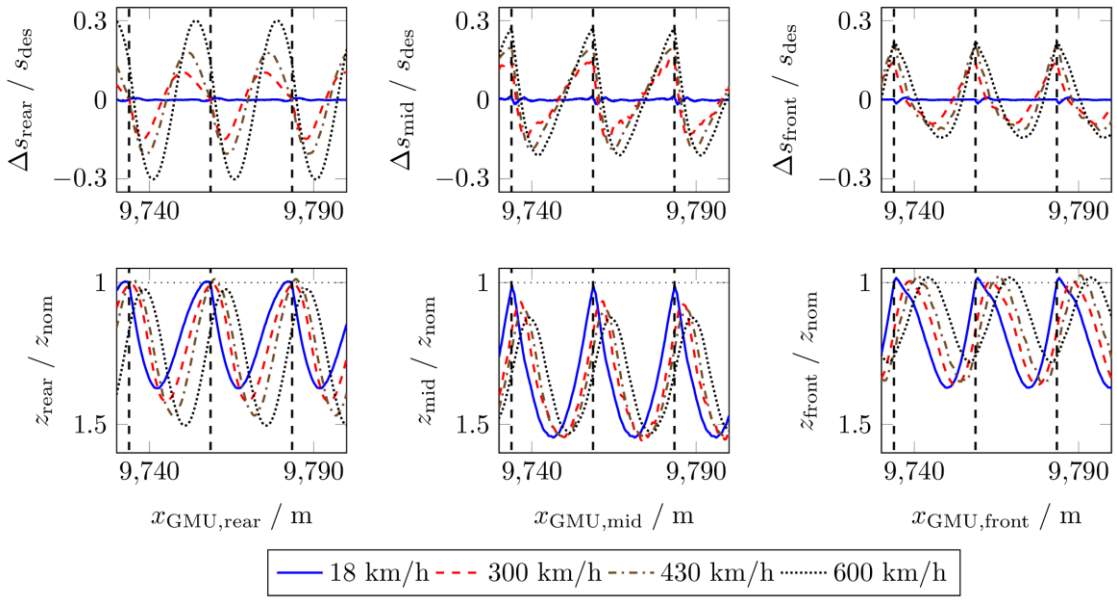

Fig. 8. Relative air gap control error and normalized absolute magnet z-positions at GMUs of magnets at the very rear end, in the middle, and at the very front end of the vehicle, respectively. Vertical dashed lines mark the positions where one guideway element ends and the next one begins.

overshoots and oscillations approximately represent a step response of the system. That means, higher vehicle speeds result in stronger overshoots and oscillations of the beam inducing vibrations to the vehicle. Therefore, higher guideway stiffness is recommended to simplify the control task for such high velocities. However, this increases the effort for guideway production, which emphasizes the necessity of a tradeoff between acceptable effort and acceptable guideway elasticity still manageable by the control scheme.

B. Control Accuracy and Magnet Vibration

The second aspect analyzed is the air gap control accuracy and the magnet motion at three different positions along the vehicle and for different velocities. Both quantities must be considered together, because the control task is a compromise between keeping the air gap in a safe range and at the same time reducing the magnet motion to improve the ride comfort. The first row of Fig. 8 shows the relative air gap control error $\Delta s/s_{\mathrm{des}} = (s_{\mathrm{meas}} - s_{\mathrm{des}})/s_{\mathrm{des}}$ at the rear end, in the middle, and at the front end of the vehicle, respectively, with the measured air gap s_{meas} and the desired air gap s_{des}. In the second row, the normalized absolute magnet motion z/z_{nom} is plotted with the nominal magnet z-position z_{nom} being at s_{des} below the undeformed beam.

Both the air gap control error and the phase shift of the magnet motion with respect to the guideway deflection grow with increasing vehicle speed at all three considered positions. One reason for this is more severe oscillations of the beam as observed in Fig. 7. Another effect to be observed is that the largest air gap control errors occur at the vehicle's rear end, while the best control accuracy is reached at the front. A similar image is drawn by the magnet motion, which is smallest at the vehicle front. This effect can be explained by looking at the guideway deflection at the respective positions along the vehicle. While the vehicle front always enters an undeflected, resting beam, the magnets in the middle and at the rear end enter a deformed and oscillating beam. Thus, the difference of the slopes of adjacent beams is smaller at the vehicle front meaning a more severe kink for the controller to deal with at the middle and at the rear end. Besides, the absolute guideway deflection is smaller at the vehicle front, since it still increases while the vehicle front passes the beam. Therefore, the vehicle rear end seems to be the most critical part regarding potential contact of vehicle and guideway, because there the biggest deviations from the desired air gap occur. Nevertheless, the air gaps are still in a safe range even for the simulations with high velocity, which confirms the good performance of the MPC control scheme used here.

C. Influence of Guideway Stiffness

Finally, the influence of the guideway stiffness on the air gap control error and the magnet motion is investigated. Therefore, Young's modulus E is varied from 75 % to 150 % of the reference value E_0, which represents the first generation of concrete guideway at the TVE as used for the simulations described previously. In the first row of Fig. 9, the maximum relative air gap control error $\max(|\Delta s|)/s_{\mathrm{des}}$ corresponding to the first row of Fig. 8 is plotted over different vehicle velocities at the rear end, middle, and front end of the vehicle. Analogously, the second row of Fig. 9 shows the amplitude of magnet motion $\Delta z = z_{\max} - z_{\min}$ with $z_{\max}$ and $z_{\min}$ being the maximum and minimum, respectively, of the magnet z-position as shown in the second row of Fig. 8. The values for the combination of $v = 600$ km/h and $E/E_0 = 75$ % are not plotted because the simulation becomes unstable shortly after the beginning.

Due to decreasing guideway deflections for higher stiffness values, the maximum air gap control error and the amplitude of magnet motion decrease as well with increasing guideway

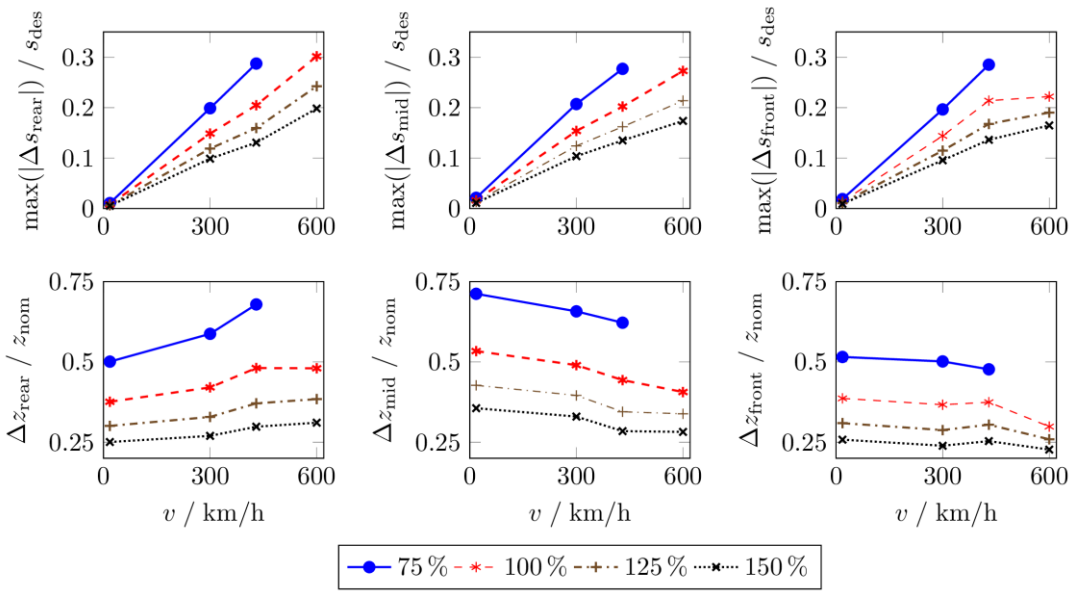

Fig. 9. Maximum air gap control error and amplitude of vertical magnet motion at the very rear end, in the middle, and at the very front end of the vehicle, respectively, for different guideway elasticity values E/E_0 plotted over different velocities.

stiffness. At the rear end, the effect of elasticity variation on the magnet motion is the stronger the higher the vehicle speed is. A different behavior can be observed at the front end, where elasticity variation has an equal effect for all velocities except for 600 km/h, for which the effect is even smaller. The reason for this observation lies in the guideway oscillations. While the vehicle leaves the beam, the bending decreases and an overshoot occurs while the rear end is still on the beam, see Fig. 7. Thus, the guideway oscillations are more severe at the rear end than in the middle and at the front end.

VII. Conclusions

For high-speed maglev systems, dealing with the dynamic bending of the guideway girders of elevated tracks under the load of the vehicle is a challenging task for the magnet controller. The air gap between vehicle and guideway must be kept in a non-critical range to avoid contact. Therefore, stiff girders would be preferable to minimize the deflections. However, high guideway stiffness brings along increased production effort and material consumption. Dynamics simulations of traveling high-speed maglev vehicles can contribute to address this dilemma and find a tradeoff.

In this contribution, the concept of moving system boundaries is applied and implemented to construct a regularly pillared elastic guideway of infinite length. The methods and results published in [6] and [7] are summarized here. Hermite polynomials are used to obtain guideway deflections at arbitrary positions of the girder by interpolating nodal coordinates. The same polynomials are used to distribute magnetic forces to adjacent nodes by calculating equivalent nodal forces and torques. The vehicle is modeled as a two-dimensional rigid multibody system on the basis of a Transrapid vehicle with three sections and 76 mechanical degrees of freedom. Together with a physically advanced magnet model and a model predictive control scheme ensuring stable levitation, vehicle and guideway dynamics are analyzed for different vehicle speeds and guideway elasticities.

In general, the intensity of overshoots and oscillations of the guideway girders increases with increasing vehicle velocity resulting in stronger air gap control errors and magnet vibrations. At the rear end of the vehicle, the largest deviations from the desired air gap occur, making it the most critical position along the vehicle concerning the control task, which is a remarkable result. However, the obtained results are uncritical for all simulated scenarios. Investigations regarding stiffness variations of the guideway girders show that higher stiffness would be advantageous for the dynamic situation all along the vehicle. However, its influence is smaller in the middle and at the front than at the rear end of the vehicle.

Due to the modular setup of the presented simulation model, further investigations can be done with little effort like analyzing the influence of other magnet models, various control approaches, or differently parameterized guideway elements.

References

[1] K. Popp and W. Schiehlen, "Dynamics of Magnetically Levitated Vehicles on Flexible Guideways", *Proceedings of IUTAM Symposium on the Dynamics of Vehicles on Roads and Railway Tracks*, pp. 479–503, Swets and Zeitlinger, 1976.

[2] R. Meisinger, "Simulation of Maglev Vehicles Riding Over Single and Double Span Guideways", *Mathematics and Computers in Simulation*, vol. 21, pp. 197–206, Elsevier, 1979.

[3] R. Meisinger, "Simulation of a Single and Double-Span Guideway under Action of Moving MAGLEV Vehicles with Constant Force and Constant Gap", *Sonderdruck Schriftenreihe der Georg-Simon-Ohm-Fachhochschule Nürnberg*, vol. 14, 2002.

[4] N. Hägele and F. Dignath, "Vertical Dynamics of the Maglev Vehicle Transrapid", *Multibody System Dynamics*, vol. 21, pp. 213–231, 2009.

[5] M. Dellnitz, F. Dignath, K. Flaßkamp, M. Hessel-von Molo, M. Krüger, R. Timmermann and Q. Zheng, "Modelling and Analysis of the Nonlinear Dynamics of the Transrapid and Its Guideway", *Progress in Industrial Mathematics at ECMI 2010*, vol. 17, pp. 113–123, Springer, 2012.

[6] G. Schneider, X. Liang, F. Dignath and P. Eberhard, "Simulation of the Maglev Train Transrapid Traveling on a Flexible Guideway Using the Multibody Systems Approach", *ECCOMAS Multibody Dynamics 2019. Computational Methods in Applied Sciences*, vol. 53, pp. 502–510, Springer, 2020.

[7] G. Schneider, P. Schmid, F. Dignath and P. Eberhard, "Modeling and Simulation of a High-speed Maglev Vehicle on an Infinite Elastic Guideway", *Proceedings of the 10th ECCOMAS Thematic Conference on Multibody Dynamics*, pp. 420–431, Budapest University of Technology and Economics, 2021.

[8] T. Kurz, P. Eberhard, C. Henninger and W. Schiehlen, "From Neweul to Neweul-M^2: Symbolical Equations of Motion for Multibody System Analysis and Synthesis", *Multibody System Dynamics*, vol. 24, pp. 25–41, 2010.

[9] S. Ren, A. Romeijn and K. Klap, "Dynamic Simulation of the Maglev Vehicle/Guideway System", *Journal of Bridge Engineering*, vol. 15, pp. 269–278, American Society of Civil Engineers, 2010.

[10] K. Popp and W. Schiehlen, "Ground Vehicle Dynamics", Springer, 2010.

[11] B. Klein, "FEM: Grundlagen und Anwendungen der Finite-Element-Methode im Maschinen- und Fahrzeugbau (in German)", Springer Vieweg, 2015.

[12] P. Schmid, G. Schneider, F. Dignath, X. Liang and P. Eberhard, "Static and Dynamic Modeling of the Electromagnets of the Maglev Vehicle Transrapid", *IEEE Transactions on Magnetics*, vol. 57, pp. 1–15, 2021.

[13] G. Schneider, P. Schmid, F. Dignath and P. Eberhard, "Coupled Vehicle-Guideway Dynamics Simulations of the Transrapid With Discretized Levitation Magnet Forces", *Proceedings of the 10th European Nonlinear Dynamics Conference*, 2022.

[14] P. Schmid and P. Eberhard, "Offset-free Nonlinear Model Predictive Control by the Example of Maglev Vehicles", *IFAC-PapersOnLine*, vol. 54, pp. 83–90, 2021.